ISSN 0006-2979, Biochemistry (Moscow), 2020, Vol. 85, No. 11, pp. 1458-1467. © Pleiades Publishing, Ltd., 2020.
Published in Russian in Biokhimiya, 2020, Vol. 85, No. 11, pp. 1718-1728.

Investigation of Allosteric Effect of 2,8-Dimethylation of A2503 in *E. coli* 23S rRNA by Molecular-Dynamics Simulations

T. M. Makarova[1,a]* and G. I. Makarov[1]

[1]*South Ural State University, 454080 Chelyabinsk, Russia*
[a]*e-mail: makarovatm@susu.ru*

Received June 15, 2020
Revised October 1, 2020
Accepted October 2, 2020

Abstract—Ribosome is a molecular machine that synthesizes all cellular proteins. It also is a target of about half of the clinically used antibiotics. Adaptive chemical modification of ribosomal RNAs residues is one of the ways to provide resistance to certain antibiotics. A curious example of such modification is 2,8-dimethylation of A2503 in 23S rRNA, which induces resistance to phenols, linkosamides, oxazolidinones, pleuromutilins, and certain macrolides. In this article the effect of 2,8-dimethylation of A2503 on conformation and mobility of RNA residues of the 70S *E. coli* ribosome was investigated employing molecular dynamics simulations method. Significant alterations were detected both in the immediate environment of the 2503 23S rRNA residue and in the nucleotides located deeper in the nascent peptide exit tunnel (NPET), which are known to be involved in signal transmission from the antibiotics bound in the NPET to the peptidyl transferase center. These alterations shift the ribosome towards the A/A, P/P-state from the conformationally different state – P/P, E/E one in our case. The obtained results allow us to conclude that the effect of m^2m^8A2503 modification involves additional stabilization of the A/A, P/P-state favoring the peptidyl transferase reaction (PTR) contrary to antibiotics that inhibit PTR.

DOI: 10.1134/S0006297920110139

Keywords: ribosome, resistance, antibiotics, A2503, molecular dynamics

INTRODUCTION

Ribosome is a large ribonucleoprotein complex that synthesizes all cellular proteins according to the program delivered by messenger RNA. Being one of the key elements of a living cell, this ancient molecular machine contains universally conserved structural elements built from ribosomal RNA (rRNA) that relatively rarely mutate under natural conditions [1]. This circumstance along with the existence of multiple copies of ribosomal RNA gene in genomes of living organisms made the ribosome a logical target for a variety of antibiotics [2]. Approximately half of the antibiotics used today in the clinical practice are inhibitors of protein synthesis on the ribosome. Nevertheless, the number of pathogenic microorganisms resistant to ribosomal antibiotics is growing every year [2, 3].

The mechanism of bacterial ribosome resistance to antibiotics is usually realized via chemical modifications of rRNA residues, predominantly concentrated in the ribosome functional centers [4], and these modifications comprise an additional nonconstitutional methylation of one or another rRNA residue [5]. An example of this is methylation of the A2503 residue (hereafter, the *E. coli* numbering is used for rRNA) of the 23S rRNA in the large subunit of bacterial ribosome at C8 position, carried out by the Cfr methyltransferase [6], first discovered in *S. sciuri* [7] and belonging to the so-called radical SAM-methyltransferases family 1 [8]. In the wildtype bacterial ribosome, the A2503 residue is also subjected to post-transcriptional constitutive methylation at C2 position by the RlmN methyltransferase; the combined action of these methyltransferases results in 2,8-dimethylation of the A2503 residue and its transformation into the m^2m^8A2503 residue.

The additional chemical modification provides bacterial resistance to antibiotics from different families (phenicols, linkcosamides, oxazolidinones, pleuromutilins and streptogramines A) termed $PhLOPS_a$ resistance according to the first letters of the names of antibiotic families involved [9]. Emergence of such a pronounced multidrug resistance in the ribosome is usually explained

Abbreviations: MD, molecular dynamics; NPET, nascent peptide exit tunnel; PTC, peptidyl transferase center.

* To whom correspondence should be addressed.

through the direct steric clashes imposed by the additional methyl group of the m^2m^8A2503 residue preventing antibiotic binding (see, for example, [10]). However, it must be mentioned that the structures of the ribosome with dimethylated A2053 residue have not been elucidated yet, and the detailed structural analysis of the ribosome complexes with antibiotics has not been performed.

The conserved m^2A2503 residue connects two single-stranded rRNA regions that form the so-called tunnel walls. Here the m^2A2503 residue is wedged into the nucleotide chain between A2059 on the one side and G2061 on another one, while A2060 is outlooped from the stack. This chain of 2058-2062 23S rRNA residues is assumed to be a pathway for signals transmission from the interior sites of the NPET up to the PTC [11-13].

To investigate the effect of A2503 dimethylation on conformations of RNA residues, we employed the molecular dynamics (MD) simulations method, which was successfully applied to describe dynamic aspects of the bacterial ribosome structure and functioning [13]. The effect of m^2A2503 8-methylation was investigated both for the ribosome in A/A, P/P-state preceding the peptidyl transferase reaction (PTR), and in the P/P, E/E-state, which, according to several data, was allosterically antagonistic to the first state [14, 15].

Models of the complexes of the entire 70S *E. coli* ribosome in both functional states with two variants of A2503 residue methylation were prepared for following simulation. The effect of the resistance modification on the conformation and non-covalent bonds of the rRNA residues was studied, and the greatest conformational changes were found in the residues U2609 and U1782 spatially separated from A2503, and they also were found even deeper down the NPET around the A751 residue. All these residues, according to the experimental data, participate in some cases of RT–PTC signal transmission when the allosteric communication is interrupted by antibiotics along with stalling peptides, and these residues are associated with m^2m^8A2503 through a network of non-covalent interactions.

MATERIALS AND METHODS

Modeling systems. The *E. coli* ribosome structure obtained by cryoelectron microscopy with 2.9 Å resolution (PDB code: 5AFI) [10] was chosen as an initial construct for the modeling systems. The missing modified bases were added to the ribosome complex with deacylated E–$tRNA^{fMet}$, fMet–P–$tRNA^{fMet}$, and Phe–A/T–$tRNA^{Phe}$ as part of the triple complex with EF–Tu, GTP, and kirromicyn in accordance with the information from the databank [16].

Earlier, we already described the procedure for obtaining ribosome complexes from the 5AFI structure that stably and reproducibly were able to bind tRNAs at both the A/A- and P/P-sites and at the P/P- and E/E-sites [17]. Here we only mention that this procedure contained at least three short MD simulations with consecutive removal of the positional restraints from various parts of the system. Systems with m^2m^8A2503 were made on their basis, and MD simulations for them were preceded by energy minimization by combining the fastest descent method with the Broyden–Fletcher–Goldfarb–Shanno method with limited use memory [18].

Molecular dynamic conditions and protocol. All MD simulations and analysis of the resulting trajectories were performed using the GROMACS [19, 20] package version 5.1.4 and the AMBER-14SB force field [21].

Topologies, geometry optimization, and molecular electrostatic potentials of noncanonical RNA residues and amino acid residues associated with the 3′-end of tRNA were obtained by quantum-chemical calculations. Prior geometry optimization of a newly parametrizing residue was carried out with PRIRODA software [22, 23] by DFT method with mPBE functional [24] and L1 basis set [25]. Optimization continued until either 300 steps were completed or gradient reached the value less than 10^{-6} Hartree/Bohr. Final geometry optimization of the residue and its molecular electrostatic potential calculation were performed with FIREFLY package [26, 27] via the Hartree–Fock method with 6-31G* basis. Optimization was also terminated either when 300 steps were completed or gradient reached the value less than 10^{-6} Hartree/Bohr.

All molecular dynamics simulations were performed at 310 K (*E. coli* temperature optimum) with a coupling time of 0.1 ps under the control of a velocity scaling thermostat with an additional stochastic term [28] and periodic boundary conditions with an isotropic constant pressure maintained by the Berendsen barostat [29] with 5 ps coupling time. Electrostatic interactions were processed using the Ewald particles network [30] with 0.125 nm grid step and the fourth order of interpolation. The simulated system was centered in an orthorhombic cell with edges of $24 \times 27 \times 25$ nm, filled with TIP4Pew water molecules in order to separate the borders of the ribosome by the solvent layer of at least 1.5 nm depth from the cell boundaries. Negative charge of the system was neutralized by potassium ions with improved Van-der-Waals parameters [31], together with structural magnesium ions visible by cryoelectron microscopy. 100 mM KCl and 6 mM $MgCl_2$ in the form of ions were also added to the neutralized system.

Integration time step in all the simulations was 2 fs; the coordinates were written to the trajectory file every 15 ps.

Methods of analysis of MD trajectories. Analysis of non-covalent bonds and conformations of RNA residues were carried out for trajectories spans beginning from 100 ns, when RMSD (Fig. 1) and potential energy (Fig. 2) of the ribosome became stabilized.

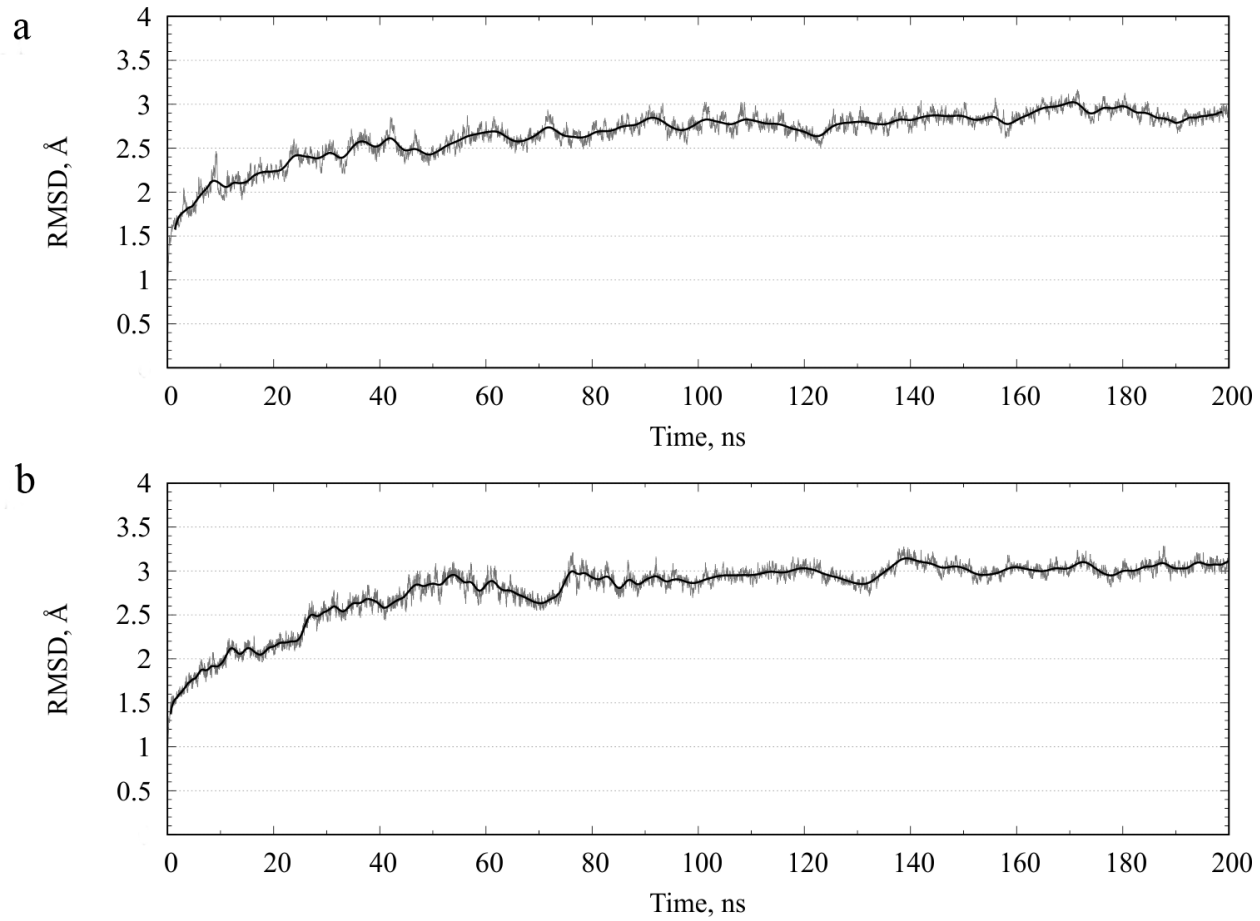

Fig. 1. Changes in the RMSD of the ribosome during molecular dynamics simulations after introduction of the modified m^2m^8A2503 residue to the system: an example of one of 4 trajectories 200 ns long for each type of system. The immediate data are shown in pale-grey on a background, running averages over 100 points are presented as a black solid line with Bezier spline. a) A/A, P/P-state. a) P/P, E/E-state.

Hydrogen bonds were analyzed using the built-in GROMACS option: in each frame of the trajectory, the presence or absence of a defined hydrogen bond was determined by geometric parameters:

- the donor atom of the hydrogen and the acceptor atom were separated by a distance of no more than 3.5 Å;
- angle hydrogen–donor–acceptor was less than 30°.

Geometric parameters were also applied to recognize stacking interactions of the nucleobases of RNA residues, for which purpose the centers of the nucleobases were calculated (the average coordinates of the atoms C2, C4, and C6 for pyrimidines and N1, N3, and C8 for purines) as well as the plane equation for these three points. Stacking interactions in the frame were detected if:

1. the distance between the centers did not exceed 5.5 Å;

2. the angle between the planes of nucleobases did not exceed 30°;

3. the angle between the plane of the first nucleobase and the segment connecting the geometric centers of both the nucleobases was at least 45°; without this condition, a coplanar base pair (e.g., Watson–Crick) would be erroneously recognized as a pair with stacking interaction.

RESULTS AND DISCUSSION

Non-constitutive methyl group of 2503 residue enhanced its stacking interactions with neighboring nucleobases. The m^2A2503 residue of the 23S rRNA situated in the strand between the H89 and H90 helical structures wedges into the stack of residues of a similar single-chain strand between H73 and H74 with formation of the unpaired stack C2063–G2061–m^2A2503–A2059–A2058. At the same time, A2060 residue from the main strand also outloops and forms tertiary stacking interactions with G2502 – the neighbor nucleobase for the investigated m^2A2503.

We started from the systems and trajectories of the following types obtained in our previous work [17] to introduce the modification m^2m^8A2503 into them and study its conformational effect on its environment, each

of which is hereafter mentioned in the form of an abbreviation. These abbreviations designate the following:

- PE – a ribosome complex with fMet–P–tRNA^{fMet} and deacylated E–tRNA^{fMet};
- AP – a ribosome complex with Ala–A–tRNA^{Phe} and fMet–P–tRNA^{fMet}.

Producing of the original AP and PE systems is described in detail in our previous work [17]. On the basis of these systems 4 200-ns long trajectories were obtained for each functional state of the ribosome. After the methyl group was added to the residue 2503 23S rRNA at the 8th position, the system quickly reached a stable state: RMSD growth saturated at 60-80 ns (Fig. 1), and oscillations of the ribosome potential energy (Fig. 2) almost immediately exhausted any directional drift.

Therefore, as in previous simulations of the AP and PE systems with the canonic m^{2}A2503, the last 100 ns of each trajectory were used for analysis. The occurrences of hydrogen bonds and stacking interactions of the rRNA residues in the obtained trajectories were extracted from the last 100 ns with calculation of the average and standard deviation for 4 values of each type of the system.

The most immediate effect of the modification was an increase in the stacking interaction occurrence of the m^{2}m^{8}A2503 base with its neighbors – G2061 and A2059 residues (Fig. 3). This slight alteration in the residue conformations and interaction strength entailed total destruction of the stacking interaction between adjacent G2502 and A2060 residues, resulting in the alternative interaction of the latter preferably with U1255 (table).

In addition, stabilization of the 2503 residue conformation and redistribution of electron density in it contributes to a significant increase in the occurrence of its hydrogen bond with the adenine of the A2062 residue, completely eliminating any cases of the A2062 incorporation between G2061 and C2063 residues, which often occurs in the frames of the A,A/P,P-state ribosome.

However, the described induced alterations involve only the closest neighbors of the 2503 residue and do not spread down the NPET or up to the PTC. Thus,

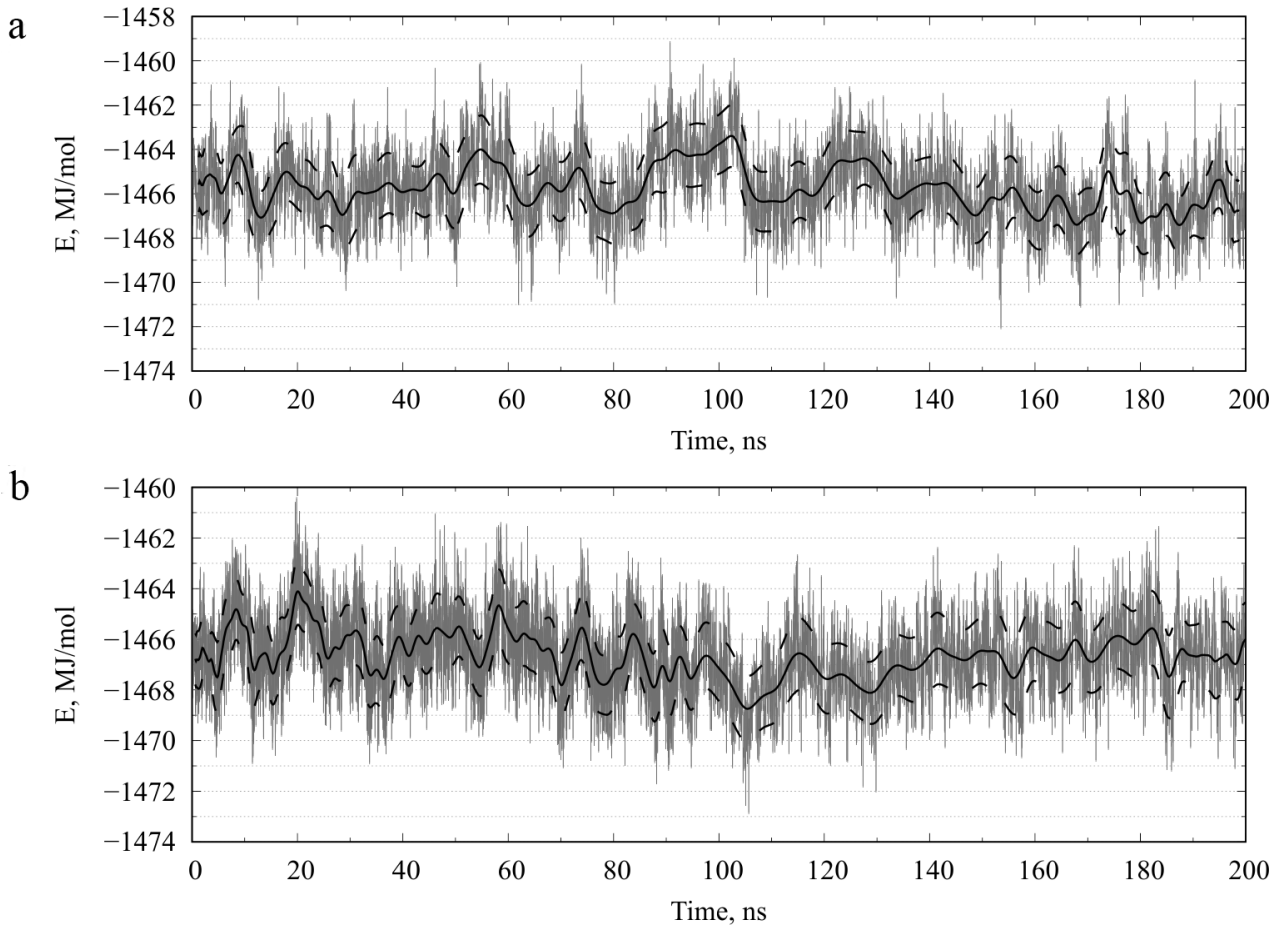

Fig. 2. Evolution of the potential energy of the ribosome during the MD simulations after introduction of the modified m^{2}m^{8}A2503 residue to the system: an example of one of 4 trajectories 200 ns long for each type of the system. The immediate data are shown in pale-grey on a background, running averages over 100 points are presented as a black solid line with Bezier spline, value ranges inside the running standard deviations are constrained by dashed lines. a) The A/A, P/P-state. b) The P/P, E/E-state.

The stably and reproducibly changing bonds in the 23S rRNA as a result of 8-methylation of the m^2A2503 residue

Bond	AP wildtype	AP m^2m^8A2503	AP wildtype	PE m^2m^8A2503
G2061‖m^2A2503	33.8 ± 25.4	38.0 ± 33.5	15.4 ± 17.4	84.6 ± 3.8
A2062/N^6–H...m^2A2503/N^7	8.3 ± 9.6	55.8 ± 40.5	37.3 ± 36.1	12.4 ± 24.9
Most important alterations in the A,A/P,P-state				
A2060‖G2502	33.0 ± 23.0	7.3 ± 14.4	26.9 ± 33.9	0.1 ± 0.2
U1255‖A2060	34.5 ± 30.8	55.4±19.5	23.1±28.1	21.6 ± 32.6
G830/N^1–H...A2448/N^7	44.6 ± 12.0	0.1 ± 0.3	0 ± 0	0 ± 0
C961‖A2031	0.2 ± 0.3	38.8 ± 19.7	72.7 ± 2.2	61.1 ± 15.4
C2499/N^4–H...G2454/O^6	6.1 ± 7.1	70.5 ± 45.7	13.8 ± 11.4	22.0 ± 20.6
G2454/N^2–H...C2499/O^2	3.5 ± 7.1	67.6 ± 41.7	0 ± 0	0 ± 0
G2454/N^1–H...C2499/N^3	3.4 ± 6.7	68.9 ± 45.1	0 ± 0	0 ± 0
A2453/N^6–H...U2500/O^4	7.0 ± 14.1	89.8 ± 5.0	0 ± 0	1.9 ± 3.2
U2500/N^3–H...A2453/N^1	8.0 ± 15.9	62.6 ± 37.4	0 ± 0	12.5 ± 17.5
G2454‖G2455	90.4 ± 11.9	19.2 ± 35.9	93.4 ± 2.6	89.1 ± 4.0
Ψ2504/N^1–H...G2447/O^6	14.8 ± 12.4	61.9 ± 31.4	0 ± 0	0 ± 0
Cm2498/N^4–H...C2499/N^3	0 ± 0	20.6 ± 3.6	0.8 ± 1.6	0 ± 0
Cm2498‖C2499	37.4 ± 11.8	72.5 ± 19.5	84.5 ± 12.4	78.8 ± 23.4
A945/N^6–H...A2448/N^3	25.7 ± 13.5	0 ± 0	0 ± 0	0 ± 0
U2500‖Ψ2504	13.3 ± 7.9	66.2 ± 22.6	1.4 ± 2.8	10.0 ± 18.0
G830‖A945	70.0 ± 7.8	20.1 ± 34.8	0.1 ± 0.2	0.3 ± 0.3
G2446/N^2–H...D2449/O^2	12.6 ± 4.0	41.5 ± 23.8	84.5 ± 6.4	61.6 ± 42.6
C2452/N^4–H...Ψ2504/O^2	3.8 ± 7.5	56.1 ± 26.4	25.6 ± 48.2	48.2 ± 40.5
Alterations in the PE-state in the NPET				
A1783/N^6–H...A2587/$O_{2'}$	7.4 ± 14.8	5.1 ± 10.2	23.1 ± 32.2	68.0 ± 6.0
U1779/N^3–H...G2588/$O_{2'}$	13.0 ± 13.1	9.7 ± 9.8	64.1 ± 42.9	0.5 ± 0.6
A1785/N^6–H...U1779/O^4	0 ± 0	0 ± 0	81.3 ± 9.0	20.1 ± 22.1
A783/$O^{2'}$–H...U1779/O^2	39.8 ± 27.0	32.2 ± 22.2	62.0 ± 41.5	0.1 ± 0.1
A751‖A789	0 ± 0	0.1 ± 0.3	33.0 ± 29.5	0 ± 0.1
U1782‖U2609	94.8 ± 4.5	92.1 ± 9.0	84.4 ± 13.7	40.1 ± 30.0
A781/$O^{2'}$–H...C1788/O^2	3.3 ± 4.0	2.8 ± 2.6	1.1 ± 2.2	23.0 ± 17.1

Table (Contd.)

Bond	AP wildtype	AP m^2m^8A2503	AP wildtype	PE m^2m^8A2503
Alterations in the P/P, E/E-state around the E-site				
U2075/N^3–H...A2435/N^1	1.5 ± 3.0	0 ± 0	6.1 ± 5.6	52.5 ± 29.5
U2074/N^3–H...G2597/N^3	0 ± 0	0 ± 0	38.3 ± 11.2	61.4 ± 5.7
U200/N^3–H...G248/$O_{4'}$	8.3 ± 16.6	6.9 ± 10.2	69.0 ± 8.5	44.1 ± 9.9
U2076‖U2596	79.3 ± 13.7	66.5 ± 19.7	60.7 ± 7.5	32.1 ± 4.6
A197/N^6–H...A2430/$O_{2'}$	57.9 ± 8.0	64.0 ± 19.1	52.8 ± 35.4	4.1 ± 4.3
U2431/$O_{2'}$–H...A2433/N^7	0 ± 0	0 ± 0	54.4 ± 20.9	8.1 ± 13.0
G2436/N^2–H...U2074/O^4	0 ± 0	0 ± 0	6.5 ± 7.8	48.7 ± 23.3
U2075/N^3–H...A2077/N^7	88.1 ± 12.2	95.2 ± 2.2	58.3 ± 9.1	21.5 ± 22.1
A2077/N^6–H...U2075/O^4	31.7 ± 47.0	0.1 ± 0.1	98.5 ± 0.4	54.0 ± 41.4
A2435/N^6–H...U2075/O^4	0 ± 0	0 ± 0	0 ± 0	38.6 ± 35.8

Note. AP and PE denote ribosome with A/A- and P/P- or P/P- and E/E-tRNA, respectively. The values are calculated from four independent trajectories for each of the systems and are presented as an average value ± standard deviation. Ellipsis denotes a hydrogen bond, double vertical bar ‖ – stacking interactions.

m^2m^8A2503 modification does not significantly perturb the A/A, P/P-state of the ribosome except the immediate vicinity of the dimethylated residue.

Remote conformational alterations in the NPET and other sites of the ribosome induced by the introduction of m^2m^8A2503. As it was described above, non-constitutive resistance methylation of the A2503 residue increased its stacking interactions. This effect was found to be transmitted deeper along the NPET, where the nascent peptide chain was expected to interact with the ribosome, and the most prominent differences were found for the P/P, E/E-state of the ribosome.

The structure formed by the stacking interactions of C2063–G2061–m^2A2503–A2059–A2058 nucleobases is transformed into the H73 helix, starting with G2057–C2611 and G2057–C2612 pairs. They are connected by covalent bonds with important allosteric sensors in the NPET, namely C2610 and U2609 [32]. In the A/A, P/P-state these residues in the NPET retain their conformation regardless of the degree of modification of A2503. However, in the P/P, E/E-state the U2609 and U1782 stacking interaction diverged via turning the U1782 residue to a position similar to that in the A/A, P/P-state of the ribosome (Fig. 4).

The turn of U1782 is transmitted to U1781 and A752 residues, also connected by stacking interactions. This shifted the A751 residue to a state that reproduced the A/A, P/P-state conformation like for the U1782 residue (Fig. 5). This resulted into complete disintegration of the stacking interaction between A751 and A789 nucleobases, similarly to the case observed in the A/A, P/P-state. Thus, only in the P/P, E/E-state, which is functionally opposite to the A/A, P/P-state, conformational alterations are detected in the NPET, and they reproduce the allosterically antagonistic state of the ribosome. This could indicate local hyperstabilization of the A/A, P/P-state by the resistance modification.

Furthermore, the U2609 and U1782 residues along with the A751 region are involved in the transmission of the allosteric signal from NPET to PTC and A site, which comprises the key mechanism of the action of antibiotics that bind in the NPET of the ribosome [32].

With regards to the other sites of the ribosome, alterations in the NPET did not induce large-scale global reconfiguration of non-covalent bonds in the rRNA, in the manner that it was observed, for example, in the case of mutations that severely affected function of the ribosome (see [17]). Stable and reproducible changes of the non-covalent RNA bonds occurrences by at least 20% were found in 253 cases for the A/A, P/P-state and 296 cases for the PE-state (in the presence of approximately 22 thousand bonds reproducibly existed in at least one of the states). The changing bonds were distributed throughout the whole ribosome, and in both cases, formed at least two large clusters, inside which the rRNA residues forming such bond were separated from each other by no more

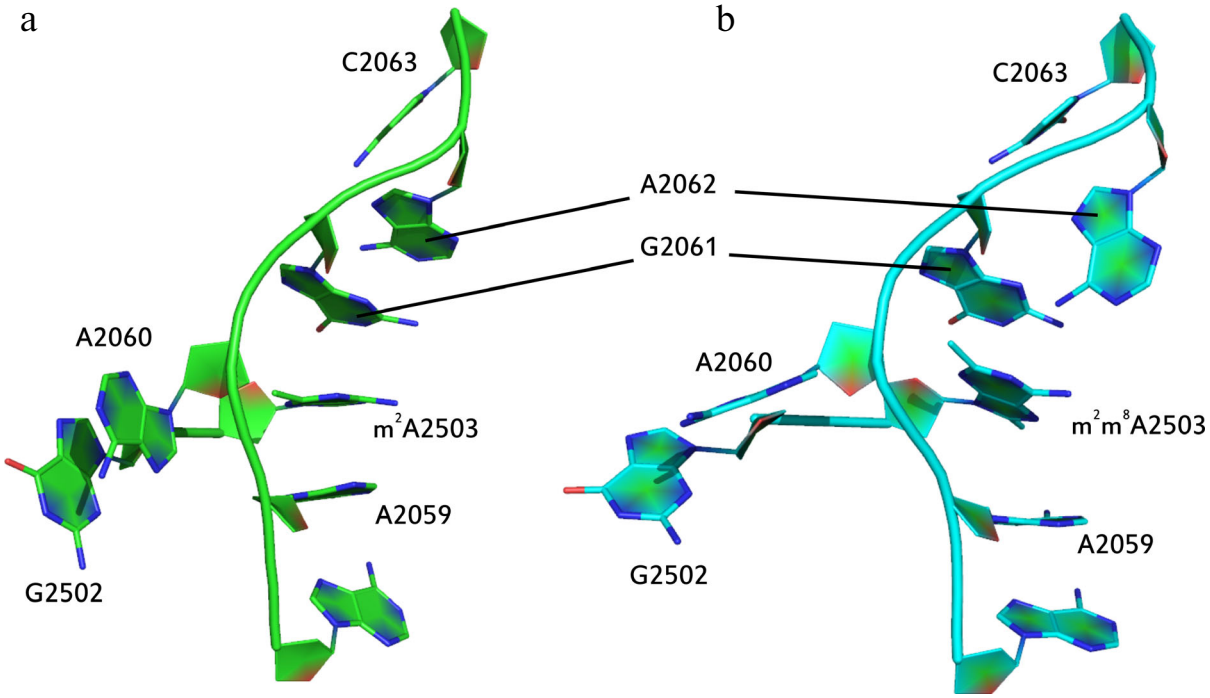

Fig. 3. Comparison of the characteristic conformation of the vicinity of A2503 residue of 23S rRNA with different modifications. Additional 8-methylation of the m^2A2503 residue reinforced stacking interactions of 2503 residue but resulted into destruction of G2502 interaction with A2060. The displayed trajectory frame is the closest to the centroid of the main cluster for coordinates of the depicted rRNA residues in 4 final 100 ns spans of 200 ns trajectories for each the system. a) A/A, P/P-state of the wild-type ribosome (with m^2A2503). b) A/A, P/P-state of the ribosome with m^2m^8A2503. (Colored versions of Figs. 3-5 are available in online version of the article and can be accessed at: https://www.springer.com/journal/10541)

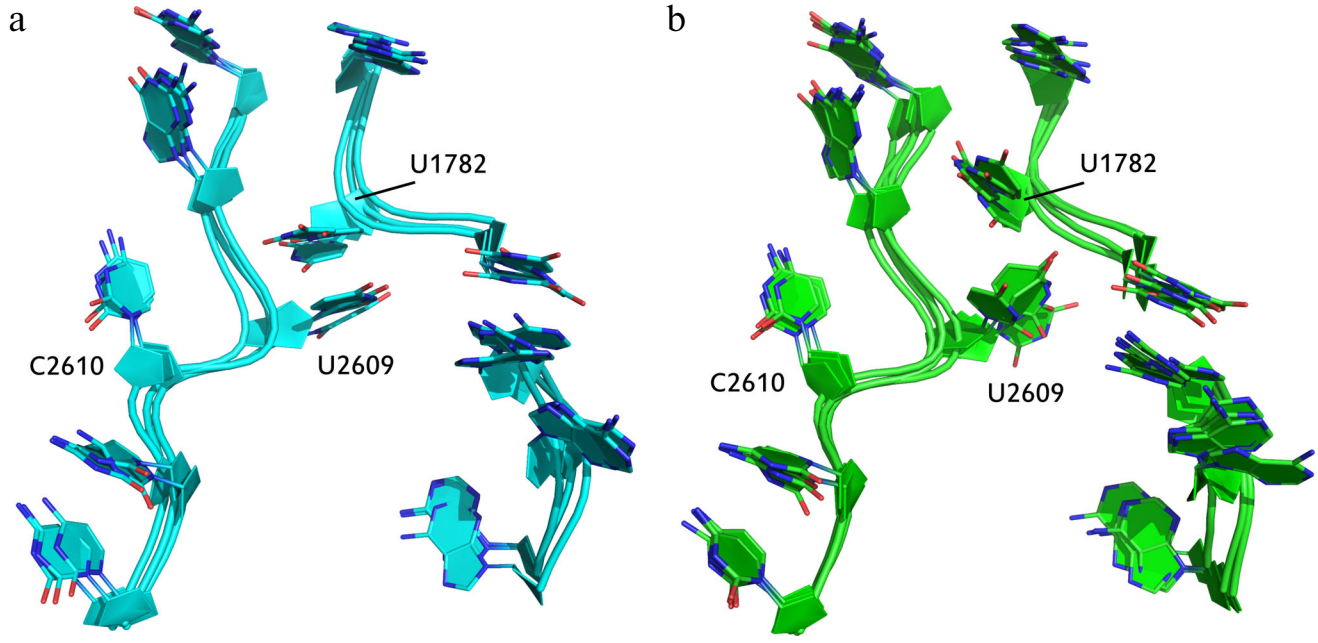

Fig. 4. Disintegration of the stacking interaction between U2609 and U1782 residues of the 23S rRNA in trajectories with 2,8-dimethylated A2503. The figure displays several most populated clusters of the NPET residues: 3 clusters for the wildtype ribosome which occupy 82.1% of all frames form 4 trajectories and 4 clusters for the ribosome with m^2m^8A2503, which contain 83.5% frames, respectively. a) P/P, E/E-state of the wild-type ribosome (with m^2A2503). b) P/P, E/E-state of the ribosome with m^2m^8A2503.

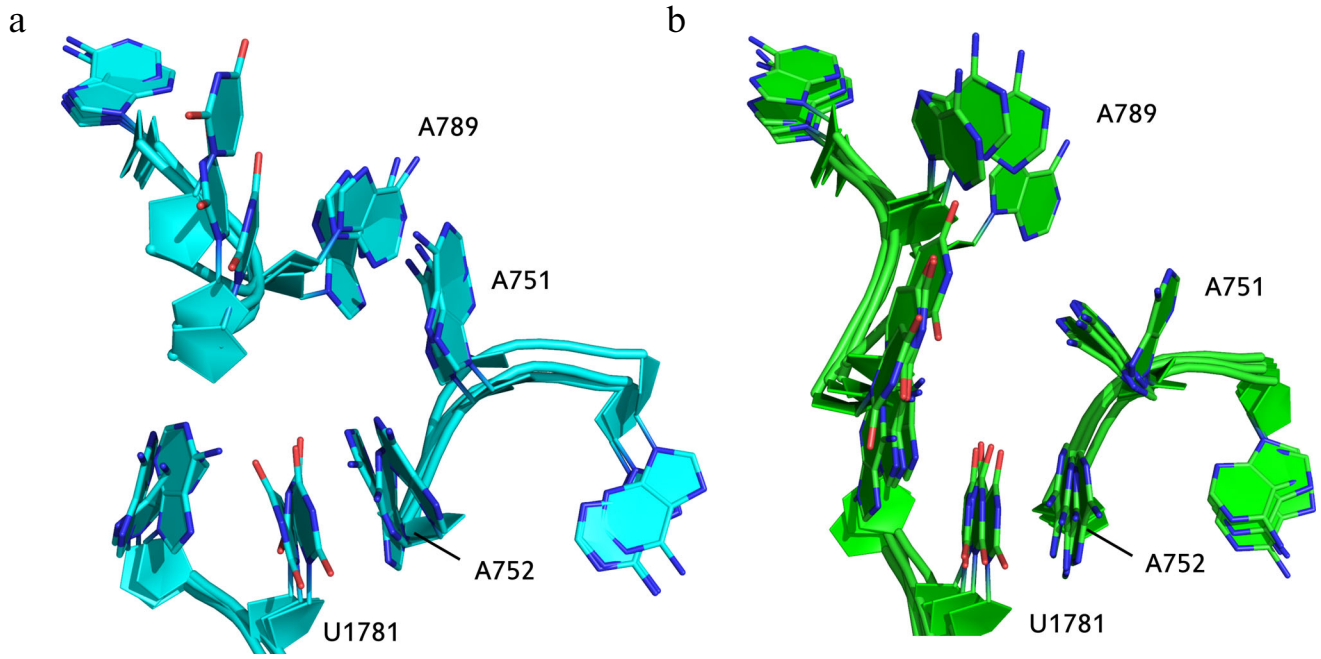

Fig. 5. Disintegration of the stacking interaction between A751 and UA789 residues of the 23S rRNA in trajectories with 2,8-dimethylated A2503. The figure displays several most populated clusters of the NPET residues: 3 clusters for the wildtype ribosome which occupy 82.1% of all frames form 4 trajectories and 4 clusters for the ribosome with m^2m^8A2503, which contain 83.5% frames, respectively. a) P/P, E/E-state of the wild-type ribosome (with m^2A2503). b) P/P, E/E-state of the ribosome with m^2m^8A2503.

than three residues in the network of stable noncovalent bonds. The first cluster contained 23S and 5S rRNA regions in the large ribosomal subunit, and the second one was comprised by fragments of the small subunit and several intersubunit bridges.

In the first cluster of rRNA residues, the largest amount of alterations in the A/A, P/P-state upon the m^2m^8A2503 modification was found around the PTC in the H89 and H74 helices, as well as the in the site of their junction, and, moreover, near the region connecting H37 and H39 helices. The detected alterations were in general related to stabilization of the internal bonds of helices and interhelical elements (table, section "Most important alterations in the AP-state").

On the contrary, in the P/P, E/E-state, the bonds redistribution was concentrated around the universally conserved joint of the H74, H75 and H93 helices (table, section "Alterations in the PE-state around the E-site"), which was adjacent to the E-tRNA C75 residue binding site – the putative allosterically sensitive site associated with E-tRNA (see [17]). The H93 hairpin from the mentioned joint is the most immediate connection between the E-site and the upper part of the NPET. It is likely that the alterations at one of its termini also induce the turn of the stack of two bases, U2609 and U1782, towards the conformation that resembles the one specific to the A/A, P/P-state.

Quantitative data about the occurrences of the noncovalent bonds discussed above are given in table.

CONCLUSION

Molecular dynamics simulations of the ribosome systems with constitutive and non-constitutive methylation of the A2503 23S rRNA residue revealed that additional 8-methylation strengthened stacking interactions of the A2503 nucleobase. This alteration drew residues G2061 and A2059 to the A2503 residue. As a result, in the A/A, P/P-state of the ribosome preceding the PTR only several significant conformational alterations and rearrangements were found in the very point of the modification. On the contrary, in the presence of tRNA in the E-site conformational rearrangements occurred both in the E-site and in the NPET involving the residues that were known to be important for allosteric connection between the NPET and the PTC.

Thus, the m^2m^8A2503 modification did not perturb the A/A, P/P-state of the ribosome required for the PTR, but shifted conformations of the certain residues in the antagonistic state back closer to the one observed in the A/A, P/P-state. Therefore, the fact that this modification protect bacteria from a wide spectrum of antibiotics with different binding sites could be explained by the additional stabilization of the pre-transpeptidational state of the ribosome. This fact should be taken into consideration in the further investigations of the effect of modifications on antibiotic- and peptide-dependent ribosome stalling.

Acknowledgments. The authors express their gratitude to Doctor of Sciences, Professor, full member of the Russian Academy of Sciences Alexey Alexeevich Bogdanov for initiation of the molecular-dynamics investigations of resistance modifications in ribosomes. The authors are grateful to the Lomonosov Moscow State University Supercomputer Center for the opportunity to carry out MD simulations using the "Lomonosov – II" supercomputer.

Funding. This research was financially supported by the Russian Science Foundation (project no. 18-74-00022) and by the Government of the Russian Federation (resolution no. 211 dated 16.03.2013, contract no. 02.A03.21.0011).

Ethics declarations. The authors declare no conflicts of interest in financial or any other sphere. This article does not contain any studies involving human participants or animals performed by any of the authors.

REFERENCES

1. Yonath, A. (2009) Ribosome: an ancient cellular nanomachine for genetic code translation, in *Biophysics and the Challenges of Emerging Threats* (Puglisi, J. D., ed.) Springer, Netherlands, pp. 121-155, doi: 10.1007/978-90-481-2368-1_8.
2. Mankin, A. (2001) Ribosomal antibiotics, *Mol. Biol.*, **35**, 509-520.
3. McCusker, K. P., and Fujimori, D. G. (2012) The chemistry of peptidyltransferase center-targeted antibiotics: enzymatic resistance and approaches to countering resistance, *ACS Chem. Biol.*, **7**, 64-72, doi: 10.1021/cb200418f.
4. Wilson, D. N. (2014) Ribosome-targeting antibiotics and mechanisms of bacterial resistance, *Nat. Rev. Microbiol.*, **12**, 35-48, doi: 10.1038/nrmicro3155.
5. Vester, B., and Long, K. S. (2009) Antibiotic resistance in bacteria caused by modified nucleosides in 23S ribosomal RNA, in *DNA and RNA Modification Enzymes: Structure, Mechanism, Function and Evolution* (Grosjean, H. ed.) Landes Bioscience, Austin, USA.
6. Giessing, A. M. B., Jensen, S. S., Rasmussen, A., Hansen, L. H., Gondela, A., Long, K., Vester, B., and Kirpekar, F. (2009) Identification of 8-methyladenosine as the modification catalyzed by the radical SAM methyltransferase Cfr that confers antibiotic resistance in bacteria, *RNA*, **15**, 327-336, doi: 10.1261/rna.1371409.
7. Schwarz, S., Werckenthin, C., and Kehrenberg, C. (2000) Identification of a plasmid-borne chloramphenicol-florfenicol resistance gene in *Staphylococcus sciuri*, *Antimicrob. Agents Chemother.*, **44**, 2530-2533, doi: 10.1128/aac.44.9.2530-2533.2000.
8. Yan, F., LaMarre, J. M., Rohrich, R., Wiesner, J., Jomaa, H., Mankin, A. S., and Fujimori, D. G. (2010) RlmN and Cfr are radical SAM enzymes involved in methylation of ribosomal RNA, *J. Am. Chem. Soc.*, **132**, 3953-3964, doi: 10.1021/ja910850y.
9. Smith, L. K., and Mankin, A. S. (2008) Transcriptional and translational control of the *mir* operon, which confers resistance to seven classes of protein synthesis inhibitors, *Antimicrob. Agents Chemother.*, **52**, 1703-1712, doi: 10.1128/AAC.01583-07.
10. Fischer, N., Neumann, P., Konevega, A. L., Bock, L. V., Ficner, R., Rodnina, M. V., and Stark, H. (2015) Structure of the *E. coli* ribosome–EF–Tu complex at <3Å resolution by Cs-corrected cryo-EM, *Nature*, **520**, 567-570, doi: 10.1038/nature14275.
11. Makarov, G., Golovin, A., Sumbatyan, N., and Bogdanov, A. (2015) Molecular dynamics investigation of a mechanism of allosteric signal transmission in ribosomes, *Biochemistry (Moscow)*, **80**, 1047-1056, doi: 10.1134/S0006297915080106.
12. Vázquez-Laslop, N., Ramu, H., Klepacki, D., Kannan, K., and Mankin, A. S. (2010) The key function of a conserved and modified rRNA residue in the ribosomal response to the nascent peptide, *EMBO J.*, **29**, 3108-3117, doi: 10.1038/emboj.2010.180.
13. Sanbonmatsu, K. (2012) Computational studies of molecular machines: the ribosome, *Curr. Opin. Struct. Biol.*, **22**, 168-174, doi: 10.1016/j.sbi.2012.01.008.
14. Gnirke, A., Geigenmuller, U., Rheinberger, H. J., and Nierhaus, K. H. (1989) The allosteric three-site model for the ribosomal elongation cycle. analysis with a heteropolymeric mRNA, *J. Biol. Chem.*, **264**, 7291-7301.
15. Chen, C., Stevens, B., Kaur, J., Smilansky, Z., Cooperma, B. S., and Goldman, Y. E. (2011) Allosteric vs. spontaneous exit-site (E-site) tRNA dissociation early in protein synthesis, *Proc. Natl. Acad. Sci. USA*, **108**, 16980-16985, doi: 10.1073/pnas.1106999108.
16. Cannone, J. J., Subramanian, S., Schnare, M. N., Collett, J. R., D'Souza, L. M., et al. (2002) The comparative RNA web (CRW) site: an online database of comparative sequence and structure information for ribosomal, intron, and other RNAs, *BMC Bioinform.*, **3**, 1-31, doi: 10.1186/1471-2105-3-2.
17. Makarova, T., and Bogdanov, A. (2019) Allosteric regulation of the ribosomal A site revealed by molecular dynamics simulations, *Biochimie*, **167**, 179-186, doi: 10.1016/j.biochi.2019.09.019.
18. Byrd, R., Lu, P., and Nocedal, J. (1995) A limited memory algorithm for bound constrained optimization, *SIAM J. Sci. Comput.*, **16**, 1190-1208.
19. Van der Spoel, D., Lindahl, E., Hess, B., Groenhof, G., Mark, A. E., and Berendsen, H. J. C. (2005) Gromacs: fast, flexible, free, *J. Comput. Chem.*, **26**, 1701-1718, doi: 10.1002/jcc.20291.
20. Hess, B., and Kutzner, C., van der Spoel, D., and Lindahl, E. (2008) Gromacs 4: algorithms for highly efficient, load-balanced, and scalable molecular simulation, *J. Chem. Theory Comput.*, **4**, 435-447, doi: 10.1021/ct700301q.
21. Maier, J. A., Martinez, C., Kasavajhala, K., Wickstrom, L., Hauser, K. E., and Simmerling, C. (2015) ff14SB: improving the accuracy of protein side chain and backbone parameters from ff99SB, *J. Chem. Theory Comput.*, **11**, 3696-3713, doi: 10.1021/acs.jctc.5b00255.
22. Laikov, D. N., and Ustynyuk, Y. A. (2005) PRIRODA-04: a quantum-chemical program suite. New possibilities in the study of molecular systems with the application of parallel computing, *Russ. Chem. Bull.*, **54**, 820-826.
23. Laikov, D. N. (2011) A new parametrizable model of molecular electronic structure, *J. Chem. Phys.*, **135**, 134120, doi: 10.1063/1.3646498.

24. Adamo, C., and Barone, V. (2002) Physically motivated density functionals with improved performances: the modified Perdew–Burke–Ernzerhof model, *J. Chem. Phys.*, **116**, 5933-5940, doi: 10.1063/1.1458927.
25. Laikov, D. N. (2005) A new class of atomic basis functions for accurate electronic structure calculations of molecules, *Chem. Phys. Lett.*, **416**, 116-120, doi: 10.1016/j.cplett.2005.09.046.
26. Schmidt, M. W., Baldridge, K. K., Boatz, J. A., Elbert, S. T., Gordon, M. S., et al. (1993) General atomic and molecular electronic structure system, *J. Comput. Chem.*, **14**, 1347-1363, doi: 10.1002/jcc.540141112.
27. URL: http://classic.chem.msu.su/gran/firefly/index.html.
28. Bussi, G., Donadio, D., and Parrinello, M. (2007) Canonical sampling through velocity rescaling, *J. Chem. Phys.*, **126**, 014101, doi: 10.1063/1.2408420.
29. Berendsen, H., Postma, J., van Gunsteren, W., DiNola, A., and Haak, J. (1984) Molecular dynamics with coupling to an external bath, *J. Chem. Phys.*, **81**, 3684-3690, doi: 10.1063/1.448118.
30. Darden, T., York, D., and Pedersen, L. (1993) Particle mesh Ewald: an *nlog*(*n*) method for Ewald sums in large systems, *J. Chem. Phys.*, **98**, 10089, doi: 10.1063/1.464397.
31. Joung, I. S., and Cheatham, T. E. (2008) Determination of alkali and halide monovalent ion parameters for use in explicitly solvated biomolecular simulations, *J. Phys. Chem. B*, **112**, 9020-9041, doi: 10.1021/jp8001614.
32. Vázquez-Laslop, N., Ramu, H., and Mankin, A. (2011) Nascent peptide-mediated ribosome stalling promoted by antibiotics, in *Ribosomes: Structure, Function, and Dynamics* (Rodnina, M. V., Wintermeyer, W., Green, R., eds), published by Springer-Verlag, Wien, pp. 377-392.